Pinning of domain walls in thin ferromagnetic films

V. Jeudy,* R. Díaz Pardo, and W. Savero Torres
Laboratoire de Physique des Solides, Université Paris-Sud, Université Paris-Saclay, CNRS, UMR8502, 91405 Orsay, France

S. Bustingorry
CONICET, Centro Atómico Bariloche, 8400 San Carlos de Bariloche, Río Negro, Argentina

A. B. Kolton
CONICET and Instituto Balseiro (UNCu), Centro Atómico Bariloche, 8400 San Carlos de Bariloche, Argentina

(Received 3 October 2017; revised manuscript received 13 June 2018; published 7 August 2018)

We present a quantitative investigation of magnetic domain-wall pinning in thin magnets with perpendicular anisotropy. A self-consistent description exploiting the universal features of the depinning and thermally activated subthreshold creep regimes observed in the field-driven domain-wall velocity is used to determine the effective pinning parameters controlling the domain-wall dynamics: The effective height of pinning barriers, the depinning threshold, and the velocity at depinning. Within this framework, the analysis of results published in the literature allows for a quantitative comparison of pinning properties for a set of magnetic materials in a wide temperature range. On the basis of scaling arguments, the microscopic parameters controlling the pinning: The correlation length of pinning, the collectively pinned domain-wall length (Larkin length), and the strength of pinning disorder are estimated from the effective pinning and the micromagnetic parameters. The analysis of thermal effects reveals a crossover between different pinning length scales and strengths at low reduced temperatures.

DOI: 10.1103/PhysRevB.98.054406

I. INTRODUCTION

A major source of hysteresis in ferromagnets [1] is the pinning of magnetic domain walls (DWs), which impedes their free motion when driven by an applied magnetic field or a spin current. For a strong pinning, the DWs follow the shape of material defects, and magnetization reversal results from percolation processes of magnetic domains [2]. Weak random pinning also results in important effects: The competition with DW elasticity and thermal activation produces stochasticity [3], domain-wall roughness [4,5], and dramatically modifies the driven dynamics at small fields and currents [4,6,7].

Weak pinning may result from spatial fluctuations of domain-wall energy associated with inhomogeneous thickness in ultrathin metallic films [4] or the concentration of magnetic atoms in ferromagnetic semiconductors [8]. As pinning impedes reaching the high velocity flow regimes, several attempts have been proposed to reduce the pinning strength finding low pinning materials [9] and to engineer the pinning properties using light-ion irradiation [9–13] in ultrathin films or coupling with another magnetic layer [14].

Interestingly, the engineering of pinning is also important for superconducting materials [15,16], and a large variety of methods was developed to enhance the pinning strength on vortices. Understanding of the pinning of elastic objects, among which domain walls in thin ferromagnets is a paradigmatic example, is thus of broad interest.

How weak pinning and thermal fluctuations affect the glassy dynamics of domain walls is a critical issue for potential applications based on the controlled motion of domain walls [17,18] and for understanding the physics of phenomena as the interaction of spin current with the DW or the contribution of the Dzyaloshinskii-Moriya interaction to DW dynamics [19]. However, going beyond qualitative comparisons between pinning properties of different materials remains challenging. A quantitative framework would be particularly welcomed for a better understanding of DW pinning in thin ferromagnetic films.

The pinning-dependent DW dynamics combines both universal and material-dependent behaviors, which are not straightforward to disentangle. A depinning magnetic-field threshold H_d separates the pinning-dependent thermally activated so-called creep regime ($H < H_d$) from the depinning transition ($H \geqslant H_d$) and the flow regime ($H \gg H_d$). Until now, almost all the analyses of experiments on DW dynamics in the creep regime have been based on the seminal work of Lemerle *et al.* [4]. In this paper, it was shown that the magnetic-field-driven DW dynamics can be modeled by the motion of an elastic line in a weakly disordered medium [20]. More precisely, the measured and the predicted creep exponent μ, deduced from the velocity law $v \sim \exp(H^{-\mu})$ and the roughness exponent $\zeta = 2/3$ as $\mu = (2\zeta - 1)/(2 - \zeta) = 1/4$, respectively, were found in good agreement thus attesting the universal nature of DW creep motion. However, those predictions are only valid in the limit $H \to 0$, which restricts the analysis of domain-wall motion to the low drive creep regime.

Recently, the glassy domain-wall dynamics was investigated beyond the zero drive limit, and it was shown that the

*vincent.jeudy@u-psud.fr

universal creep regime extends up to the depinning threshold [21]. The depinning transition was also found to present universal behaviors [22]. Their analysis was pushed beyond the usual asymptotic power-law variations. The universal functions describing the creep and depinning regimes could be extracted from experimental results obtained for different materials and temperatures. Moreover, it was shown that both regimes can be described self-consistently using only three parameters absorbing all the intrinsic temperature- and material-dependent pinning properties. These effective pinning parameters are an effective pinning barrier height $k_B T_d$, where k_B is the Boltzmann constant, a depinning threshold H_d and a depinning velocity v_T [22]. As the latter are directly related to the physics at the so-called Larkin regime of an elastic string in a random medium [23,24], they can be used to bridge between the nontrivial macroscopic universal behavior, such as the collective creep and depinning phenomena, to the micromagnetic level of description at which domain walls and their pinning to inhomogeneities emerge. This situation is analogous to the case of vortex pinning in superconductors where the Larkin regime bridges between the macroscopic scale and the Ginzburg-Landau continuum description for which vortices are described by well-defined pinned elastic objects [15,25].

The aim of this paper is to understand better the correlations between the material- and the temperature-dependent pinning parameters controlling the glassy DW dynamics and the microscopic origins of DW pinning. To this end we exploit the self-consistent "top-down" approach [22] described above, starting from the identification of universal features in the driven DW glassy dynamical regimes. We deduce a "map" of the material- and temperature-dependent effective pinning parameters (T_d, H_d, and v_T) controlling DW velocity. We develop a model providing scaling relations among the effective pinning parameters, the micromagnetic parameters (the saturation magnetization M_s, the domain-wall surface energy σ, the domain-wall thickness parameter Δ, and the Gilbert damping factor α), and the microscopic pinning parameters characterizing the weak pinning disorder (which are the pinning strength $f_{\rm pin}$ and the correlation length of the disorder ξ). The model is used to estimate the microscopic pinning parameters, which are not directly accessible experimentally. A strong modification of domain-wall pinning properties at low temperatures is evidenced. This paper provides a systematic quantitative analysis of magnetic domain-wall pinning.

The organization of the paper is the following. Section II discusses DW dynamics: It starts from a qualitative description and extends to the self-consistent modeling, which is used for the extraction of pinning parameters controlling creep and depinning regimes of the velocity. Section III presents a set of pinning parameters deduced from 50 velocity curves reported in the literature for different materials and temperatures and then proposes a model, which relates those parameters to microscopic properties of pinning. A comparison of microscopic parameters characterizing the pinning and an analysis of thermal effects is presented in Sec. IV. In Sec. V we overview our results and summarize our main conclusions.

II. DOMAIN-WALL DYNAMICS

After a qualitative description of different magnetic-field-driven DW dynamical regimes observed experimentally, a self-consistent empirical approach exploiting the universal features of the creep and depinning regimes, is presented. In this way we obtain the three fundamental pinning parameters which we use in the next section to compare different magnetic materials.

A. Different dynamical regimes

A typical velocity curve of the domain wall obtained for a Pt/Co/Pt ultrathin film is shown in Fig. 1 and is used to describe the different dynamical regimes. At low drive ($H < H_d$), the DWs move in the creep regime which is controlled by pinning, DW elasticity, and thermal activation. The DW velocity follows an Arrhenius law $v \sim \exp(-\Delta E/k_B T)$, where $k_B T$ is the thermal activation energy, and ΔE is the effective pinning barrier height. The creep regime presents a universal behavior. Close to zero drive ($H \to 0$), the barrier height follows a

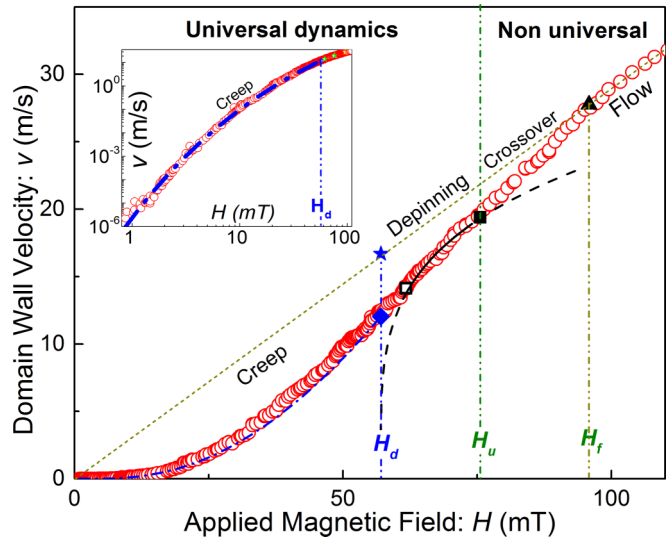

FIG. 1. Typical velocity curve observed for an ultrathin Pt/Co/Pt film at room temperature taken from Ref. [22]. The universal and the nonuniversal dynamics are separated by the boundary field H_u, which corresponds to the upper limit of the depinning transition. Within the nonuniversal dynamics, DWs present a crossover between the depinning transition and the linear flow regime, which is observed at the largest drive. Within the universal dynamics ($H < H_u$), the depinning threshold $H = H_d$ separates the creep regime ($H < H_d$) from the depinning transition ($H_d < H < H_u$). The inset: log-log plot of the velocity curve highlighting the creep regime. The dotted line in the main panel corresponds to the linear extrapolation of the flow regime, observed for $H > H_f$. The dashed-dotted curve is a fit of Eqs. (1) and (2) for the creep regime. The dashed curve is a fit of Eq. (6) for the depinning transition using the universal parameter $x_0 = 0.65$. The part that matches with experimental data is underlined by black solid segments. The diamond and star points located on the vertical line $H = H_d$ are the velocity at depinning $v(H_d)$ and the depinning velocity v_T. $v(H_d)$ corresponds to the inflection point separating the creep regime from the depinning transition. The value of v_T was deduced from Eq. (5) and is found to coincide with the flow velocity DWs would have in the absence of pinning.

power-law variation with magnetic-field $\Delta E \sim H^{-\mu}$ where μ is the so-called creep exponent [4,20]. Increasing the applied magnetic field reduces the effective barrier height which vanishes ($\Delta E \to 0$) at the depinning threshold ($H = H_d$) [21,26].

Above the threshold, the curvature of the velocity curve becomes negative ($d^2v/dH^2 < 0$) [22] (see Fig. 1). The DWs undergo a depinning transition controlled by elasticity and thermal noise, which is also a universal dynamical regime [22]. At zero temperature, the velocity is expected to follow a power-law scaling with magnetic-field $v \sim (H - H_d)^\beta$, where β is the so-called depinning exponent. At finite temperatures, the thermal activation produces a "thermal rounding" of the velocity curve. The velocity is also predicted to present an asymptotic power-law scaling with temperature at the depinning threshold $v \sim T^\psi$, where ψ is the thermal rounding exponent [22,27–31]. The end of the depinning transition corresponds to the onset of the divergence between the velocity curve and the magnetic-field scaling law which crosses over at a magnetic-field $H \simeq H_u$ (see Fig. 1). This upper boundary also roughly defines the limit of universal dynamics which covers the whole creep regime and the depinning transition [21,22]. Below $H = H_u$, the dynamics of a DW can be described as the motion of an elastic string submitted to thermal activation and to pinning [20,32] and is independent of its magnetic structure. The measured critical exponents for a DW moving in an ultrathin film are compatible with theoretical predictions ($\mu = 1/4$ [4,20,21,33], $\beta = 0.25$ [34], and $\psi = 0.15$ [22,26,29,31]) for the quenched Edwards-Wilkinson universality class with random short-range uncorrelated pinning disorder.

Above $H = H_u$, the DW dynamics is found to be of nonuniversal nature. The DW presents a crossover from the depinning transition to a flow regime. In the flow regime, the velocity depends on the time evolution of DW magnetic texture and presents a nonmonotonous variation with the magnetic field. Below the Walker limit [35] $H \leqslant H_w = (1/2)\alpha M_s$, where α is the so-called Gilbert damping parameter and M_s is the saturation magnetization, the DW is expected to follow the so-called steady-state regime for which its magnetic texture remains fixed during the motion. Above H_w the DW velocity presents a negative slope with the drive, and it recovers a linear asymptotic variation at sufficiently high drive ($H \gg H_w$) which corresponds to the so-called asymptotic precessional regime. Experimentally, the steady-state regime is rarely observed [36–38]. As the Walker field is usually much smaller than the depinning field ($H_w \ll H_d$), it is generally hidden by pinning [33]. This is the case for the curve of Fig. 1 where the linear variation corresponds to the precessional asymptotic regime [22,33].

B. Universal glassy dynamics

As shown in Refs. [21,22], the universal features of driven glassy DW dynamics, including the whole creep regime and the depinning transition, can be made explicit by introducing the reduced variables H/H_d, T/T_d, and v/v_T, where H_d, T_d, and v_T are material- and temperature-dependent parameters characterizing DW pinning. It is worth stressing that such a description is self-consistent: The velocities of depinning and creep regimes are described by universal (though very different) functions of the *same set* of three above-mentioned reduced variables. In the following, we describe the form of such functions. Table I presents an overview of parameters describing the DW dynamics.

For the creep regime [$0 < H < H_d(T)$], the DW velocity is described by an Arrhenius law,

$$v(H,T) = v(H_d,T)\exp\left(-\frac{\Delta E}{k_B T}\right), \tag{1}$$

with the effective pinning barrier height given by

$$\Delta E = k_B T_d(T)\left[\left(\frac{H}{H_d}\right)^{-\mu} - 1\right], \tag{2}$$

where $k_B T_d$ is the characteristic pinning energy scale and μ (=1/4) is the universal creep exponent. $v(H_d,T)$ corresponds to the velocity at depinning. In Ref. [21], it was shown that the ratio $\Delta E/k_B T_d$ is a universal function of the reduced magnetic-field H/H_d, (i.e., material and temperature independent) which controls the creep velocity in the whole $0 < H < H_d$ range. The asymptotic behaviors of the pinning barrier height are a power-law divergence $\Delta E \sim (H/H_d)^{-\mu}$ close to zero drive ($H \to 0$) and a linear collapse $\Delta E \sim \mu(1 - H/H_d)$ close to the depinning threshold ($H \to H_d$).

For the depinning transition [$H_d(T) < H < H_u(T)$], the combined contributions of magnetic field and temperature on the velocity are described by a generalized universal homogeneous function [28,31,39,40] of the form

$$y = g\left(\frac{x}{x_0}\right), \tag{3}$$

where the scaled dimensionless variables are defined as $y = (v/v_T)(T/T_d)^{-\psi}$ and $x = [(H - H_d)/H_d]^\beta (T/T_d)^{-\psi}$. A rather good approximation for the shape [22] of the g function is

$$g(x/x_0) = [1 + (x/x_0)^n]^{1/n}, \tag{4}$$

where n (=8.7 ± 0.4) tunes the width of the crossover and $x_0 = 0.65 \pm 0.04$ is a universal constant. The DW velocity presents two universal asymptotic power-law behaviors. At the depinning threshold ($H = H_d$), the temperature variation can be written as

$$v(H_d,T) = v_T(H_d,T)\left(\frac{T}{T_d}\right)^\psi, \tag{5}$$

where ψ (=0.15) is a depinning exponent and $v_T(H_d,T)$ is a depinning velocity. Just above the depinning threshold [22] for $H \gtrsim H_d[1 + (0.8(T_d/T)^{-\psi})^{1/\beta}]$, the velocity is dominated by the driving field as

$$v(H,T) \approx \frac{v_T(H_d,T)}{x_0}\left(\frac{H - H_d}{H_d}\right)^\beta, \tag{6}$$

where β (=0.25) is another depinning exponent. For most of the studied magnetic materials, the thermal activation energy is much smaller than the pinning energy ($T \ll T_d$), and part of the velocity curve just above H_d presents good agreement with the predictions of Eq. (6) as shown in Fig. 1.

To summarize, the set of Eqs. (1)–(3) constitutes a self-consistent description of the DW glassy dynamics observed below the universality limit ($H \leqslant H_u$). The creep motion

TABLE I. Parameters describing domain-wall dynamics, classified according to the length scale at which they emerge.

Characteristic length scale	Variable	Name
Micromagnetic continuum description	A	Stiffness energy
	K_{eff}	Anisotropy energy
	M_s	Saturation magnetization
	α	Gilbert damping factor
	γ	Gyromagnetic factor
Microscopic domain-wall scale $L < L_c$	$\Delta \sim \sqrt{\frac{K_{\text{eff}}}{A}}$	Domain-wall width parameter
DW micromagnetic structure	$\sigma \sim \sqrt{K_{\text{eff}} A}$	Domain-wall energy
	$m_{fl} = \frac{\gamma \Delta \alpha}{1+\alpha^2}$	Domain-wall mobility (flow regime)
DW pinning	D	Strength of the pinning disorder
	ξ	Correlation length of the disorder
	$f_{\text{pin}} \sim \frac{\sqrt{D}}{\xi}$	Pinning force [cf. Eqs. (14) and (15)]
Mesoscopic DW scale $L \sim L_c$	T_d	Depinning temperature [cf. Eqs. (1) and (2)]
(Larkin regime)	H_d	Depinning threshold [cf. Eqs. (1) and (2)]
	v_T	Depinning velocity [cf. Eq. (5)]
Macroscopic DW scale $L \gg L_c$	μ	Creep exponent [cf. Eq. (2)]
(*Random manifold regime*) creep regime	$\Delta E/(k_B T_d)$	Universal energy barrier function [cf. Eq. (2)]
Depinning transition	$v(H_d)$	Velocity at depinning [cf. Eqs. (1) and (2)]
	β	Depinning exponent (field effects) [cf. Eq. (6)]
	ψ	Depinning exponent (thermal effects) [cf. Eq. (5)]
	x_0	Universal metric factor [cf. Eq. (6)]
	$g(x/x_0)$	Universal function of depinning [cf. Eq. (3)]

and the depinning transition are both described by universal functions, and their asymptotic limits agree with the predictions from models of elastic lines in disordered media. The nonuniversal character of DW motion is caught by only three purely material- and temperature-dependent parameters corresponding to the depinning threshold H_d, temperature T_d, and velocity v_T.

C. Self-consistent analysis of DW dynamics

The determination of material- and temperature-dependent parameters requires to perform simultaneously a fit of the creep regime [Eqs. (1) and (2)] with adjustable velocity-magnetic-field coordinates at depinning $[H_d,\ v(H_d)]$ and of the depinning transition [Eq. (6)] over an adjustable range (with an upper bound $H = H_u$). The following procedure can be used:

(1) Step 1: The upper boundary of the creep regime $[H_d,\ v(H_d)]$ is assumed to correspond to the inflection point of the velocity curves (see the diamond in Fig. 1). Indeed, the curvature is predicted to change the sign at the depinning transition: positive for the creep regime [$H < H_d$, see Eqs. (1) and (2)] and negative for the depinning regime [$H > H_d$, see Eq. (6)].

(2) Step 2: An estimate of T_d is then deduced from a fit of $v(H)$ with Eqs. (1) and (2) (with $\mu = 1/4$) over the range of $0 < H < H_d$ (see the dot-dashed line in Fig. 1).

(3) Step 3: In order to improve the accuracy for the values of H_d and $v(H_d)$ a fit of Eqs. (1) and (2) is performed for increasing values of H. The upper boundary of the creep regime $[H_d,\ v(H_d)]$ can also be defined as the limit above which the fit and the experimental curve start to diverge. Step 2 can then be repeated to improve the accuracy for the T_d value.

(4) Step 4: A final fine-tuning of H_d and $v(H_d)$ is deduced from a fit of Eq. (6) with $\beta = 0.25$ and $x_0 = 0.65$ over the largest magnetic-field range (see the dashed curve in Fig. 1).

(5) Step 5: When the linear asymptotic precessional flow regime is observed ($H_w \ll H_d$), the coordinates $[H_d,\ v(H_d)]$ can be also finely adjusted using Eq. (5) and the observed coincidence between v_T and the velocity of the linear flow regime for Pt/Co/Pt films [22] (see the star in Fig. 1).

This procedure was used to analyze 50 velocity curves reported in the literature.

III. DOMAIN-WALL PINNING

In this section, we first present the effective pinning parameters (H_d, v_T, and T_d) deduced from the analysis of the glassy dynamics for different materials and various temperatures. We then propose a model, which relates those parameters to the micromagnetic and microscopic pinning parameters.

A. Effective pinning parameters

A synoptic presentation of the effective pinning parameters is proposed in Figs. 2 and 3. See also Table II for details and for the values of micromagnetic parameters.

A plot of the depinning field H_d versus depinning temperature T_d is shown in Fig. 2. As can be observed, the data points are rather dispersed. The values of H_d and T_d extend over two orders of magnitude (H_d: from 3 mT for CoFeB/MgO to 300 mT for TbFe and T_d: from 600 K for (Ga,Mn)(As,P) to 50 000 K for CoNi). From Fig. 2 it is not evident to extract general trends for the variations of the effective height pinning barrier $k_B T_d$ with the depinning threshold H_d. The analysis of those variations is extensively discussed in the following.

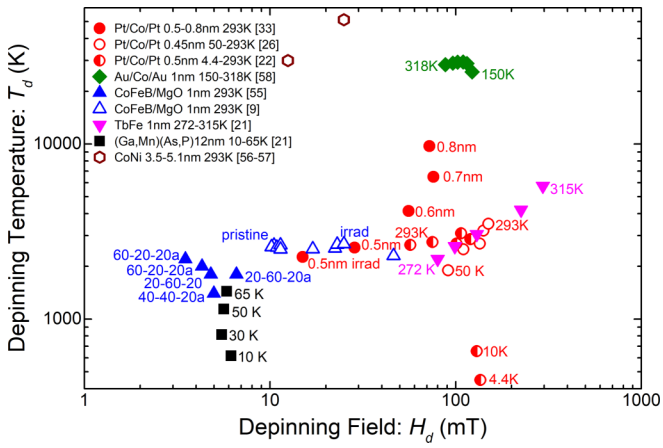

FIG. 2. Depinning temperature T_d versus depinning field H_d. For each magnetic material, the legend indicates the film thickness, the explored temperature range, and the reference. For the CoFeB films, the letter "a" means annealed.

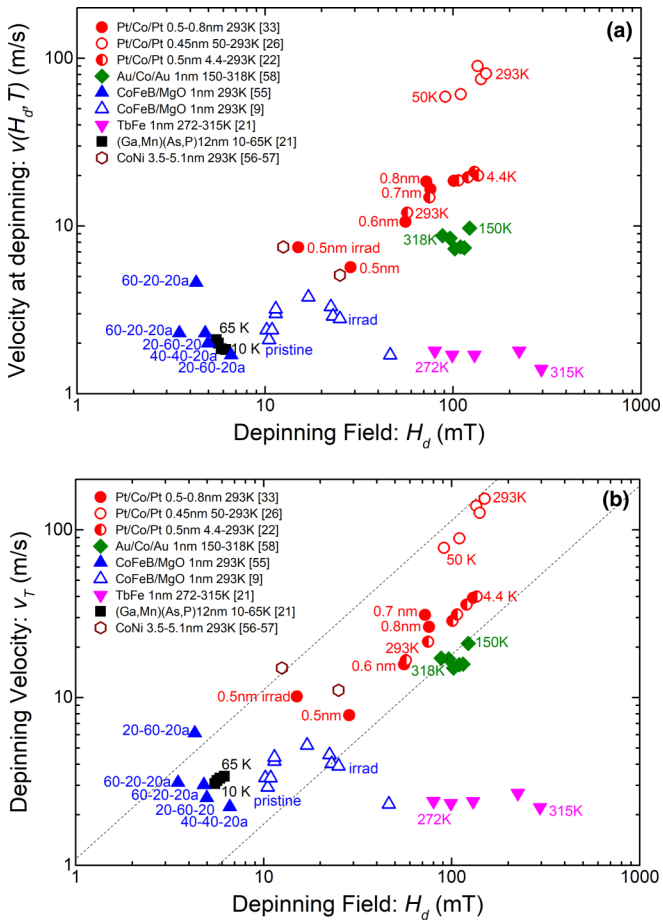

FIG. 3. (a) Velocity at depinning $v(H_d)$ and (b) depinning velocity v_T versus depinning field H_d. $v(H_d)$ corresponds to the measured upper limit of the creep velocity. $v_T(H_d)$ was deduced from Eq. (5) and is only dependent on material and temperature. The global increasing trend of $v_T(H_d)$ is materialized by two dashed lines which correspond to linear variations of depinning velocity ($v_T = mH_d$) for two constant slopes ($m = 0.15$ and $1.1\ \mathrm{m\,s^{-1}\,mT^{-1}}$). For the CoFeB films, the letter a means annealed.

Now let us discuss the results obtained for the velocity at depinning $v(H_d)$ and the depinning velocity $v_T(H_d)$ [see Eq. (5)]. As shown in Fig. 3(a), $v(H_d)$ globally increases with increasing H_d value except for some materials and covers a typical range extending from 1 to 100 m/s. The significantly lower values obtained for TbFe compared to other magnetic materials could be due to an underestimation of the depinning threshold since no change in curvature sign was observed in the velocity curve of Ref. [21]. For the depinning velocity v_T, a global increase with H_d is observed in Fig. 3(b) except for some materials. This trend can be framed by two linear variations of the depinning velocity ($v_T = mH_d$) for two constant slopes [see the dashed lines which correspond to $m = 0.15$ and $1.1\ \mathrm{m\,s^{-1}\,mT^{-1}}$].

More generally, the map of effective pinning parameters presented in Figs. 2 and 3(b) is the main result of the present paper. It serves as a starting point for the discussion on the microscopic origin of pinning proposed in the following.

B. Model for domain-wall pinning

In order to go further in the analysis of pinning properties, the effective pinning parameters deduced from velocity curves (H_d, v_T, and T_d) have to be related to the microscopic characteristics of pinning and ultimately to the micromagnetic parameters of each material.

The universal functions describing the velocity are consistent with the general theoretical predictions obtained by solving the large-scale nonequilibrium behavior of a driven elastic string in random medium [41]. We thus expect to obtain H_d, v_T, and T_d from a simple dimensional analysis of such a model at relatively short length scales. We follow the approaches of Refs. [4,42,43] which consider the DW as an elastic line not taking into account the detailed magnetic texture [44,45] and express the model parameters in terms of micromagnetic quantities.

The variation of the free energy associated with the displacement of a DW segment of length L over a transverse distance u is roughly given by

$$\delta F(L,u) = \sigma t u^2/L + \delta F_{\mathrm{pin}}(L,u) - 2M_s H t L u, \quad (7)$$

where the magnetization saturation M_s, and the DW elastic energy σ ($\approx 4\sqrt{AK_{\mathrm{eff}}}$ for a Bloch wall, where A and K_{eff} are the stiffness and the effective anisotropy constant, respectively) are micromagnetic parameters. t is the layer thickness (see Table I for an overview of the parameters controlling domain-wall pinning). In Eq. (7), the first term corresponds to the elastic energy associated with the elongation of domain-wall δF_{el}, the second is the pinning energy δF_{pin}, and the third term stands for the contribution of the driving magnetic-field δF_H.

The DW is expected to be depinned for an applied magnetic-field $H = H_d$ such that no metastable states with zero velocity exist for $H > H_d$. Larkin realized that this happens when a DW segment of a characteristic size L_c displaces over the characteristic range of the effective pinning potential ($u \approx \xi$) or pinning force correlation length in response to the field. The so-called Larkin length L_c is field independent and can be estimated from $\delta F_{\mathrm{pin}}(\xi, L_c) \approx \delta F_{el}(\xi, L_c)$. This estimate can be explicitly performed after modeling the scaling properties of

TABLE II. Material- and temperature-dependent parameters. For each material, the thickness (t) and the temperature of the experiment [T(K)] are indicated. The depinning temperature (T_d), the magnetic-field (H_d), and the domain-wall velocity at the depinning field [$v(H_d)$] are deduced from a fit of the velocity curves (see the text). m_{fl} (m s^{-1} mT^{-1}) is the best fit for the slope of the linear precessional regime. The saturation magnetization M_s, the DW energy σ, and the DW thickness parameter Δ are extracted or deduced from the references indicated below the name of material. The numbers in the parentheses are the error bars.

Material	t (nm)	T (K)	T_d (K)	H_d (mT)	$v(H_d)$ (m/s)	m_{fl} (m s^{-1} mT^{-1})	M_s (kA/m)	σ (μJ/m^2)	Δ (nm)
Pt/Co/Pt	0.5	293	2558(10)	28.5(2)	5.7(0.2)	0.276(0.005)	910	9030	6.2
Ref. [33]	0.6		4145(25)	56(1)	10.6(1.0)	0.325(0.005)	1130	11700	5.5
	0.7		6490(30)	76(1)	16.6(1.0)	0.370(0.005)	1200	10700	6.7
	0.8		9720(45)	72(1)	18.4(1.0)	0.454(0.005)	1310	10200	8.6
Irradiated	0.5		2260(50)	15(1)	7.5(1.0)	0.676(0.005)	700	3080	15.6
Pt/Co/Pt	0.45	293	1900(100)	91(4)	59(2)		800	7400	5.8
Ref. [26]		200	2500(100)	110(5)	61(2)		1120	12300	6.9
		150	2700(100)	135(5)	90(2)		1260	14700	7.3
		100	3200(100)	141(5)	75(2)		1370	16700	7.6
		50	3500(100)	150(5)	81(2)		1470	18500	7.9
Pt/Co/Pt	0.5	293	2650(50)	57(3)	12.0(0.5)	0.288(0.005)	910	9030	6.2
Ref. [22]		225	2750(50)	75(3)	14.8(0.5)	0.307(0.005)	1120	12300	6.9
		150	2700(50)	101(3)	18.6(0.5)	0.280(0.005)	1330	16000	7.5
		100	3090(50)	107(3)	18.7(0.5)	0.260(0.005)	1470	18500	7.9
		50	2860(50)	120(3)	19.5(0.5)	0.292(0.005)	1600	21000	8.2
		10	660(50)	130(3)	21.0(0.5)	0.363(0.005)	1720	23500	8.5
		4.4	450(50)	136(3)	20.0(0.5)	0.364(0.005)	1730	23700	8.5
Au/Co/Au	1.0	318	28400(1500)	88.0(1.0)	8.7(1.0)		1400		
Ref. [58]		273	29000(1500)	96.5(1.0)	8.4(1.0)		1400		
		243	29300(1500)	102.5(1.0)	7.3(1.0)		1400		
		213	29400(1500)	110.0(1.0)	7.5(1.0)		1400		
		183	28800(1500)	115.0(1.0)	7.4(1.0)		1400		
		150	25800(1000)	122.6(1.0)	9.7(1.0)		1400		
$Co_{20}Fe_{60}B_{20}$ an	1	293	1800(100)	6.6(0.2)	1.7(0.5)		1100	9200	9.7
$Co_{20}Fe_{60}B_{20}$ ag			1800(100)	4.8(0.2)	2.3(0.5)		1000	2700	30.2
$Co_{40}Fe_{40}B_{20}$ an			1400(100)	5.0(0.2)	2.0(0.5)		880	7400	10.7
$Co_{40}Fe_{40}B_{20}$ ag			2000(100)	4.3(0.2)	4.6(0.5)		1100	4900	21
$Co_{60}Fe_{20}B_{20}$ an			2200(100)	3.5(0.5)	2.3(0.5)		1100	5100	27.7
Ref. [55]									
$Co_{20}Fe_{60}B_{20}$ an	1	293							
Ref. [9]									
Dose $\times 10^{19}$ He/nm^2									
0			2640(100)	10.5(0.2)	2.1(0.5)		880		
0.1			2580(100)	10.2(0.2)	2.4(0.5)		860		
0.2			2570(100)	10.9(0.2)	2.4(0.5)		890		
0.4			2640(100)	11.4(0.2)	3.0(0.5)		760		
0.6			2500(100)	11.4(0.5)	3.2(0.5)		810		
0.8			2510(100)	17(0.2)	3.8(0.5)		840		
1			2540(100)	22.4(0.2)	3.3(0.5)		770		
1.2			2670(100)	23.0(0.2)	2.9(0.5)		710		
1.4			2680(100)	25.0(0.5)	2.8(0.5)		680		
1.6			2300(100)	46.3(0.5)	1.7(0.5)		670		
TbFe	5 × 1.8	271	5750(50)	295(5)	1.4(0.1)				
Ref. [21]		289	4200(50)	225(5)	1.8(0.1)				
		304	3050(50)	130(5)	1.7(0.1)				
		310	2600(50)	100(5)	1.7(0.1)				
		315	2200(50)	80(5)	1.8(0.1)				
(Ga,Mn)(As,P)	12	10	616(10)	6.2(0.1)	1.8(0.1)	0.537(0.005)	38	130	11.1
Ref. [21]		30	1440(20)	5.8(0.1)	1.8(0.1)	0.564(0.005)	34	100	11.6
		50	1140(20)	5.6(0.1)	2.0(0.2)	0.566(0.005)	26	60	11.7
		65	815(10)	5.5(0.1)	2.3(0.1)	0.58(0.01)	18	30	12.0
[Co/Ni] superlattice	1.1 × 3	293	51300(500)	25(1)	5.1(0.1)		930	6900	5.8
Ref. [56]									
[Co/Ni] superlattice	1.2 × 4	293	30000(10000)	12.5(2.0)	7.5(2.5)		680	8300	6.95
Ref. [57]									

$\delta F_{\rm pin}(u, L)$, typically using collective pinning theory if pinning is weak [24,25].

At depinning, the elastic and Zeeman terms are of the same order [$\delta F_{el}(L_c, \xi) \approx \delta F_H(L_c, \xi)$], establishing a connection between the collectively pinned DW segment length L_c and the depinning field H_d. Moreover, we can assume that the typical pinning energy barrier height encountered in Eqs. (2) and (5) corresponds to the pinning energy at the depinning threshold $k_B T_d \approx \delta F_{\rm pin}(L_c, \xi)$. As the latter energy contribution should be also on the same order as $\delta F_{el}(L_c, \xi)$, using Eq. (7) we obtain

$$k_B T_d = (\xi^2 \sigma t)/L_c, \tag{8}$$

$$H_d = \sigma \xi \big/ \left(2 M_s L_c^2\right), \tag{9}$$

which relate the depinning temperature and magnetic field to the microscopic length scales L_c and ξ and to the micromagnetic parameters σ and M_s.

As this model is essentially based on scaling arguments, it is expected to describe correctly the temperature variation of L_c and ξ and to provide a rough estimate of their magnitude from the knowledge of velocity response parameters T_d and H_d.

Note that the dynamics of DW magnetic texture may play a role in the physics of depinning threshold H_d as evidenced in Refs. [44,45]. The discussion of those models, which are based on an oversimplified description of DW pinning [45] or magnetic structure [44], is beyond the scope of this paper. The internal degrees of freedom of the DW is not accounted in the simple elastic line model.

Let us now discuss the DW velocity at depinning $v(H_d, T)$ and the depinning velocity v_T. In Eqs. (5) and (6), v_T is defined as a purely scaling factor, and it is important to give to this parameter a precise physical meaning. Following the discussions in Refs. [22,26], we assume that v_T corresponds to the velocity that DWs would have in the absence of pinning, which yields

$$v_T(H_d, T) = m_{fl}(H_d, T) H_d(T), \tag{10}$$

where $m_{fl}(H_d, T)$ is the mobility of the DW in the flow regime at the depinning field H_d. Strictly, $m_{fl}(H_d, T)$ has a non-monotonous field dependence with two important reference values: $m_{fl}(H_d, T) = \gamma \Delta/\alpha$ for $H_d \leqslant H_w$ and

$$m_{fl}(H_d, T) = \frac{\gamma\, \Delta\alpha}{1+\alpha^2} \tag{11}$$

for $H_d \gg H_w$, where $\Delta = \sqrt{A/K_{\rm eff}}$ is the domain-wall width parameter, α is the Gilbert damping parameter, and γ is the gyromagnetic factor ($=1.76 \times 10^{11}$ Hz T^{-1}). For the data of Refs. [21,22,33] as in the case of Fig. 1, $m_{fl}(H_d, T)$ corresponds to the mobility of the asymptotic precessional flow regime (i.e., $H_w \ll H_d$).

C. Thermal effects

The thermal activation produces fluctuation of the DW position which, if strong enough, can appreciably smooth the effective random pinning potential experienced by DWs. As a result, the correlation length of the disorder $\xi(T)$ and the Larkin length $L_c(T)$ are expected to increase with increasing temperature. For a weakly pinned elastic line, Nattermann *et al.* [42] and Chen and Marchetti [43] proposed the following temperature variations: $\xi(T) = \xi_0[1 + (T/T_d)]^3$ and $L_c(T) = L_{c0}[1 + (T/T_d)]^5$, which are interpolation formulas between power-law variations deduced from scaling arguments and values (ξ_0 and L_{c0}) corresponding to the limit of zero thermal fluctuation of the DW position. More recently, Agoritsas *et al.* [46] proposed the analytic predictions,

$$L_c(T, \xi) = \frac{4\pi}{\sigma t D^2}\left(\frac{k_B T}{f(T/T_d)}\right)^5, \tag{12}$$

and

$$\xi(T) = \frac{\sqrt{3}(4\pi)^{5/6}}{\sigma t D}\left(\frac{k_B T}{f(T/T_d)}\right)^3, \tag{13}$$

where the function f is given by the implicit equation $f^6 = 4\pi(1-f)(T/T_d)^6$. The zero-temperature values are given by

$$L_{c0} = (4\pi)^{1/6}\frac{(k_B T_d)^5}{\sigma t D^2}, \tag{14}$$

and

$$\xi_0 = \sqrt{3}(4\pi)^{5/6}\frac{(k_B T_d)^3}{\sigma t D}. \tag{15}$$

In Eqs. (12)–(15), D is the strength of disorder [46–48], reflecting the typical amplitude of the quenched random pinning potential and has the dimension of the square of an energy. Note that Eqs. (14) and (15) indicate that L_{c0} and ξ_0 are also expected to present intrinsic temperature variations due to their dependency on micromagnetic and pinning parameters. Such intrinsic variation must be hence distinguished from the extrinsic variation explicitly given in Eqs. (12) and (13), which becomes important only when the temperature T is close to T_d.

D. Pinning and domain-wall dynamics

In order to get a better insight into the variation of DW dynamics with the magnetic material and temperature, it is interesting to relate the pinning parameters (see Figs. 2 and 3) with the micromagnetic and microscopic pinning parameters.

A more intuitive insight of the predictions of Ref. [46] can be deduced from scaling arguments. Following Ref. [4] and neglecting thermal effects (i.e., $L_c = L_{c0}$ and $\xi = \xi_0$) the pinning energy can be modeled by collective pinning theory [24] $\delta F_{\rm pin}(L_{c0}, \xi_0) = f_{\rm pin}\xi_0\sqrt{n\xi_0 L_{c0}}$, where n is the density of pinning centers ($\approx 1/\xi_0^2$) and $f_{\rm pin}$ is a typical pinning force. Using Eqs. (8) and (9) leads to

$$(k_B T_d)^3 = \sigma t (f_{\rm pin}\xi_0)^2 \xi_0, \tag{16}$$

which for $f_{\rm pin}^2 \xi_0^2 = D/[\sqrt{3}(4\pi)^{5/6}]$ is equivalent to Eq. (15) and to

$$(H_d)^3 = \frac{(f_{\rm pin}\xi_0)^4}{\xi_0^7 \sigma t^4 (2M_s)^3}, \tag{17}$$

respectively. Eqs. (16), (17), (10), and (11) now fully relate the pinning parameters controlling DW dynamics (H_d, v_T, and T_d) to the micromagnetic parameters (σ, M_s, Δ, and α) and the microscopic pinning parameters ($f_{\rm pin}$ and ξ_0). Therefore, combining the description of universal behaviors

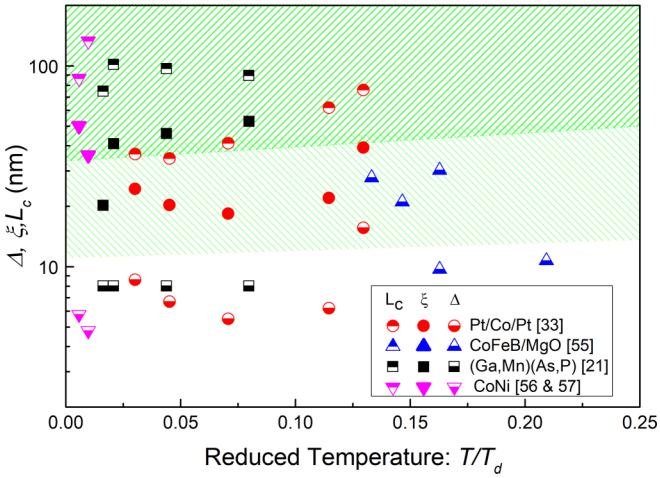

FIG. 4. Characteristic lengths versus reduced temperature. Δ, ξ, and L_c are the domain-wall width parameter, the correlation length of the disorder, and the Larkin length, respectively. The hatched areas highlight the range of variation of the three lengths.

[see Eqs. (1)–(3), (5), and (6) in Sec. II B], the predictions of model for DW pinning [see Eqs. (16) and (17)] and experimental measurements of the micromagnetic parameters, one can estimate the microscopic parameters controlling DW pinning.

IV. FUNDAMENTAL PINNING SCALES

By means of the scaling model of pinning developed in Sec. III, it is possible to discuss the fundamental pinning scales from the map [see Figs. 2 and 3(b)] of material- and temperature-dependent pinning parameters controlling domain-wall dynamics.

A. Characteristic length scales of pinning

Using Eqs. (8) and (9), we can deduce the range of the pinning potential,

$$\xi = [(k_B T_d)^2/(2M_s H_d \sigma t^2)]^{1/3}, \tag{18}$$

and the Larkin length,

$$L_c = \left[(\sigma k_B T_d)/\left(4M_s^2 t H_d^2\right)\right]^{1/3}. \tag{19}$$

Those relations are expected to provide estimations of values ξ and L_c and to reveal their temperature variation [26]. Following Eqs. (18) and (19), estimations of ξ and L_c rely on the values of M_s and σ. As can be seen in Table II, this eliminates the analysis for materials Au/Co/Au, CoFeB for different irradiation doses, and TbFe. Note that we could also consider the Larkin area $L_c\xi$ $[=(k_B T_d)/(2H_d M_s t)]$, which is independent of σ.

As can be observed in Fig. 4 for all the reported materials [Pt/Co/Pt, Co/Ni, (Ga,Mn)As, and CoFeB/MgO], the range of values for the pinning correlation length ($\xi \approx 20$–50 nm) and the Larkin length ($L_c \approx 40$–170 nm) are relatively well separated. The ratio between L_c and ξ scales the density of pinning sites along the DWs. Its relatively small values suggest that DWs pinning involves only few pinning sites (two to four) over the Larkin length. Moreover, the correlation length of the disorder is larger than the domain-wall width parameter ($\Delta \approx 5$–20 nm) except for CoFeB/MgO for which we have $\Delta \approx \xi$. This indicates that generally the weak pinning originates from fluctuations of pinning over distances longer than the domain-wall width parameter.

B. Temperature variations of the pinning strength and length scales

Let us now discuss the temperature variation of ξ and L_c. In order to compare the temperature variation for different materials and theoretical predictions we first normalize the data for each material to values of ξ_n and L_{cn}, which are assumed to be temperature independent. Those values were chosen in order for the ratios $\xi(T)/\xi_n$ and $L_c(T)/L_{cn}$ to follow the temperature

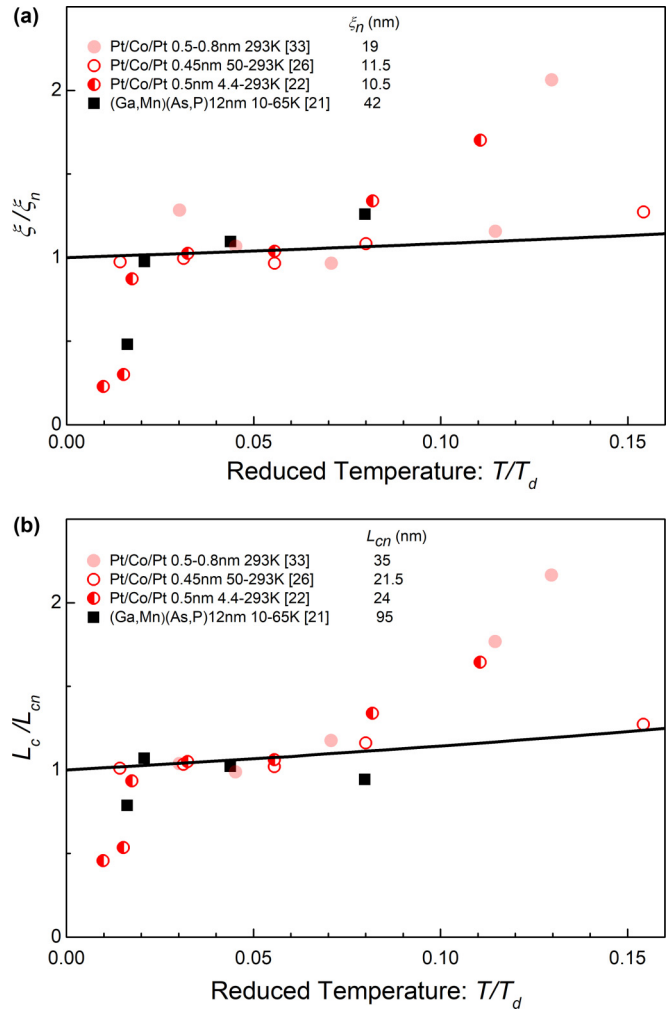

FIG. 5. (a) Reduced correlation length of the disorder ξ/ξ_n and (b) reduced Larkin length L_c/L_{cn} as a function of reduced temperature T/T_d. The solid lines in (a) and (b) correspond to the predictions of Eqs. (12) and (13), respectively. All the data correspond to single samples and variable temperatures except the shaded red points (Pt/Co/Pt: Ref. [33]), which correspond to room temperature and different sample thicknesses. The normalization values (ξ_n and L_{cn}) are indicated in the figures for each material. In the range of $0.02 < T/T_d < 0.1$, the data agree well with theoretical predictions. For $T/T_d < 0.02$, there is a drop in both ξ/ξ_n and L_c/L_{cn}.

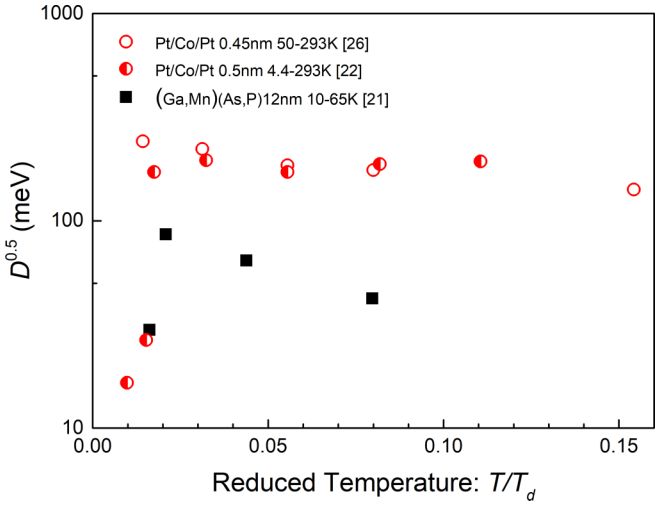

FIG. 6. Square root of the strength of the disorder as a function of reduced temperature T/T_d.

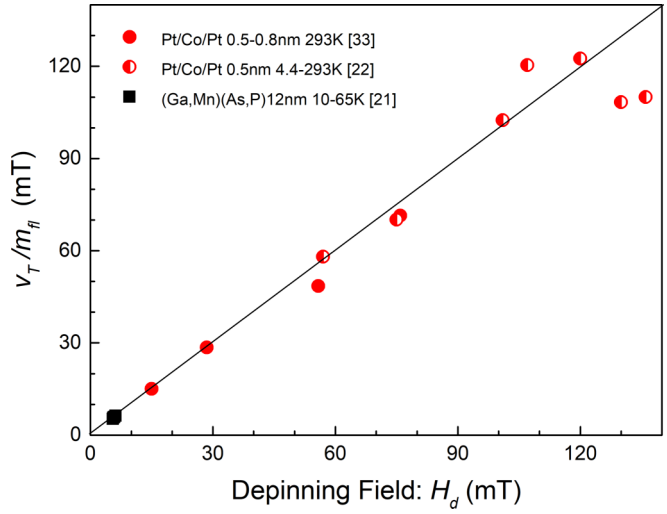

FIG. 7. Ratio between depinning velocity and mobility in the flow regime versus the depinning field. The equality between those two quantities indicates that the depinning velocity corresponds to the velocity the DW would have in the absence of pinning.

variation predicted by Eqs. (12) and (13) over the largest range of T/T_d, respectively.

The results are shown in Fig. 5 for materials for which both σ and M_s are reported in the literature. Following Eqs. (12) and (13), ξ/ξ_n and L_c/L_{cn} are predicted to decrease rather weakly as the temperature is reduced. In contrast, the experimental data present an important variation with temperature. This suggests that the thermal behavior of $\xi(T)$ and $L_c(T)$ is dominated by the temperature variation of the micromagnetic and pinning parameters of $\xi_0(T)$ and $L_{c0}(T)$ [reflected by Eqs. (14) and (15)] and not by thermal fluctuations of the DW position.

Assuming now negligible fluctuations of the DW position, the data of Fig. 5 can be viewed as the relative temperature variation of $\xi_0(T)$ and $L_{c0}(T)$. Different regimes can be clearly distinguished. For $T/T_d > 0.02$, $\xi_0(T)/\xi_n$ and $L_{c0}(T)/L_{cn}$ globally tend to weakly increase with temperature. For $T/T_d > 0.10$, the large observed fluctuations suggest a strong sample-dependent temperature behavior. For $T/T_d < 0.02$, both $\xi_0(T)/\xi_n$ and $L_{c0}(T)/L_{cn}$ are observed to drop with decreasing temperature. The decrease in $\xi_0(T)/\xi_n$ can reach a factor of 4, which suggests that $\xi_0(T)$ becomes close to the DW width Δ. Therefore, we can infer the drop observed in Fig. 5 to reflect a crossover between different pinning length scales. At sufficiently large reduced temperature ($T/T_d > 0.02$), the correlation length of the disorder is larger than the DW thickness ($\xi_0 > \Delta$). At low temperature ($T/T_d < 0.02$), the pinning is controlled by the DW width, which defines the correlation length of the disorder ($\xi_0 \approx \Delta$).

In order to further analyze the pinning, it is interesting to discuss the strength of pinning disorder. The value of the strength of the pinning disorder can be deduced from Eq. (14) $\{D^2 = (4\pi)^{1/6}[(k_B T_d)^5]/[\sigma t L_{c0}]\}$. In Fig. 6, we plot $\sqrt{D}$ (which has the dimension of an energy) as a function of the ratio T/T_d. Above the crossover ($T/T_d > 0.02$), the strength of pinning disorder is almost temperature independent for the Pt/Co/Pt films ($\sqrt{D} \approx 200$ meV) as expected for a quenched disorder. For (Ga,Mn)(As,P), the slight decrease in $\sqrt{D}$ with increasing temperature is probably associated with a not enough stringent estimation of the DW energy σ (see Table II).

For $T/T_d < 0.02$, we observe a drop in the pinning strength. At low temperatures, DWs become sensitive to pinning sites with both lower strength and shorter range, which are unefficient at higher temperatures. This also suggests the existence of different pinning strength ranges and a crossover between pinning regimes tuned by the magnitude of thermal activation. A better understanding of this issue requires further investigations.

C. Depinning velocity

Let us now discuss the depinning velocity v_T, which is important as it sets the fundamental time scale, once known as the length scales characterizing the pinning. As shown in Fig. 1, the value of v_T deduced from Eq. (5) is found to coincide with the linear extrapolation of the flow regime observed at high drive. In order to test the generality of this observation, we have analyzed the flow regime for different materials and temperatures. Table II reports the value of DW mobility m_{fl} deduced from a linear fit of the linear flow regime, which was only observed for Pt/Co/Pt and (Ga,Mn)As films. In Fig. 7, we report the variation of the ratio $v_T[(H_d, T)/m_{fl}(T)$ with the depinning field H_d. As can be observed, all the points collapse on a single line. The slope is equal to 1, which indicates that the depinning velocity can be written $v_T(H_d, T) = m_{fl}(T)H_d$. We can deduce that the depinning velocity v_T corresponds to the flow velocity that the DW would have in the absence of pinning. Following Eq. (5), this suggests that the DW velocity of the glassy dynamics scales with the domain-wall width parameter Δ and damping parameter α following Eq. (11).

V. CONCLUSION

In conclusion, we propose a quantitative and comparative study of domain-wall pinning in different ferromagnets. The latter is based on a clear discrimination between universal and material-dependent behaviors of the creep and depinning dynamical regimes. The determination of effective

pinning parameters allows to explore the interplay between micromagnetic and pinning properties of ferromagnets and domain-wall dynamics.

Our paper provides a better understanding of the microscopic origin of pinning in magnetic systems. Our analysis provides a functional dependency of DW glassy velocity with the micromagnetic and pinning parameters. This should have important implications for a comparison between experimental and theoretical studies as micromagnetic simulations on one hand [49] and to statistical models for interface motion in disordered elastic systems [46,50] on the other. In particular, the latter allows a more stringent test for the different equilibrium and depinning universality classes proposed to describe the nonequilibrium dynamics at different length scales and velocities. Moreover our analysis should help for a better understanding of the chiral effects on DW dynamics [19,51,52] and, in particular, the contribution of the Dzyaloshinskii-Moriya interaction. They should manifest through the fundamental field, temperature, and velocity scales controlling the macroscopic universal response of DWs.

ACKNOWLEDGMENTS

We wish to thank E. Agoritsas and J. Curiale for fruitful discussions, J.-P. Adam, L. Herrera Diez, D. Ravelosona, and N. Vernier for sharing their data on CoFeB. S.B. and V.J. acknowledge support by the French-Argentina Project ECOS-Sud Project No. A12E03. This work was also partly supported by the Labex NanoSaclay, Grant No. ANR-10-LABX-0035. S.B. and A.B.K. acknowledge partial support from Project No. PIP11220120100250CO (CONICET).

APPENDIX: MICROMAGNETIC AND PINNING PARAMETERS

Here, we discuss technical details on the determination of micromagnetic parameters, which are listed in Table II together with the fundamental pinning parameters controlling domain-wall dynamics. The values of magnetization saturation M_s, domain-wall energy σ, and thickness parameter Δ are directly reported from the publications when they are available or deduced from the relations $\sigma = 4\sqrt{AK_{\rm eff}}$ and $\Delta = \sqrt{A/K_{\rm eff}}$, where A is the stiffness energy and $K_{\rm eff}$ is the effective anisotropy.

For Pt/Co/Pt, the data were taken from Refs. [33] (different thicknesses t and room temperature), [26] (thickness $t = 0.45$ nm and variable temperature), and [22] (thickness $t = 0.5$ nm and variable temperature). For the 0.5-nm-thick Pt/Co/Pt film [22], the room-temperature micromagnetic parameters M_s, σ, and Δ correspond to those of the 0.5-nm-thick film of Ref. [33]. As proposed in Ref. [26], the thermal dependence of M_s was deduced from polar magneto-optical Kerr rotation. Since $A \sim [M_s(T)]^2$ and $K_{\rm eff} \sim M_s(T)$, we assumed the following temperature variations for the DW energy $\sigma \sim [M_s(T)]^{3/2}$ and the domain-wall width parameter $\Delta \sim [M_s(T)]^{1/2}$.

For Au/Co/Au, M_s was taken equal to its bulk value [53].

For (Ga,Mn)(As,P), the temperature variation of the saturation magnetization M_s was deduced from a polar magneto-optical Kerr effect measurement and was found similar to that observed for (Ga,Mn)As [36,38]. The Curie temperature is 74 ± 1 K. According to the concentration of Mn atoms, we assumed $M_s(T = 0\ {\rm K}) = 40$ kA/m [54]. The domain-wall width parameter Δ was deduced from the slope (m_{fl}) of the precessional flow regime and the prediction of the one-dimensional model: $m_{fl} = v/H = \alpha\gamma\Delta/(1+\alpha^2)$ with $\gamma = 1.76 \times 10^{11}$ Hz/T and $\alpha = 0.3$ [36,38]. The obtained value for $\Delta = 11.5 \pm 0.5$ nm is almost temperature independent and close to the value reported in Ref. [54] ($\Delta = 8 \pm 1$ nm).

For CoFeB/MgO with different Co and Fe concentrations, the data were taken from Ref. [55]. The DW energy is deduced from $\sigma = 4K_{\rm eff}\Delta$ with $K_{\rm eff} = M_s H_{k,{\rm eff}}/2$.

For CoFeB/MgO with different irradiation doses, the data were taken from Ref. [9].

For the [Co/Ni] superlattices, data were taken from Refs. [56,57]. For the DW energy, we used $\sigma = 4K_{\rm eff}/\Delta$. For the stiffness energy, we took the value ($A = 10$ pJ/m) reported in Ref. [57].

[1] A. Hubert and R. Schäfer, *Magnetic Domains* (Springer, Berlin, 1998) .
[2] J. P. Attané, Y. Samson, A. Marty, J. C. Toussaint, G. Dubois, A. Mougin, and J. P. Jamet, Phys. Rev. Lett. **93**, 257203 (2004).
[3] D.-H. Kim, S.-B. Choe, and S.-C. Shin, Phys. Rev. Lett. **90**, 087203 (2003).
[4] S. Lemerle, J. Ferré, C. Chappert, V. Mathet, T. Giamarchi, and P. Le Doussal, Phys. Rev. Lett. **80**, 849 (1998).
[5] K.-W. Moon, D.-H. Kim, S.-C. Yoo, C.-G. Cho, S. Hwang, B. Kahng, B.-C. Min, K.-H. Shin, and S.-B. Choe, Phys. Rev. Lett. **110**, 107203 (2013).
[6] J. Curiale, A. Lemaître, C. Ulysse, G. Faini, and V. Jeudy, Phys. Rev. Lett. **108**, 076604 (2012).
[7] S. DuttaGupta, S. Fukami, C. Zhang, H. Sato, M. Yamanouchi, F. Matsukura, and H. Ohno, Nat. Phys. **12**, 333 (2016).
[8] A. Lemaître, A. Miard, L. Travers, O. Mauguin, L. Largeau, C. Gourdon, V. Jeudy, M. Tran, and J.-M. George, Appl. Phys. Lett. **93**, 021123 (2008).
[9] L. Herrera Diez, F. García-Sánchez, J.-P. Adam, T. Devolder, S. Eimer, M. S. E. Hadri, A. Lamperti, R. Mantovan, B. Ocker, and D. Ravelosona, Appl. Phys. Lett. **107**, 032401 (2015).
[10] J. Ferré, V. Repain, J.-P. Jamet, A. Mougin, V. Mathet, C. Chappert, and H. Bernas, Phys. Status Solidi A **201**, 1386 (2004).
[11] F. Cayssol, J. Menéndez, D. Ravelosona, C. Chappert, J.-P. Jamet, J. Ferré, and H. Bernas, Appl. Phys. Lett. **86**, 022503 (2005).
[12] J. H. Franken, M. Hoeijmakers, R. Lavrijsen, and H. J. M. Swagten, J. Phys.: Condens. Matter **24**, 024216 (2012).
[13] S. Li, T. Amagai, X. Liu, and A. Morisako, IEEE Trans. Magn. **48**, 3658 (2012).
[14] P. J. Metaxas, R. L. Stamps, J.-P. Jamet, J. Ferré, V. Baltz, B. Rodmacq, and P. Politi, Phys. Rev. Lett. **104**, 237206 (2010).
[15] W.-K. Kwok, U. Welp, A. Glatz, A. E. Koshelev, K. J. Kihlstrom, and G. W. Crabtree, Rep. Prog. Phys. **79**, 116501 (2016).
[16] A. E. Koshelev and A. B. Kolton, Phys. Rev. B **84**, 104528 (2011).

[17] S. S. P. Parkin, M. Hayashi, and L. Thomas, Science **320**, 190 (2008).

[18] J. H. Franken, H. J. M. Swagten, and B. Koopmans, Nat. Nanotechnol. **7**, 499 (2012).

[19] S.-G. Je, D.-H. Kim, S.-C. Yoo, B.-C. Min, K.-J. Lee, and S.-B. Choe, Phys. Rev. B **88**, 214401 (2013).

[20] P. Chauve, T. Giamarchi, and P. Le Doussal, Phys. Rev. B **62**, 6241 (2000).

[21] V. Jeudy, A. Mougin, S. Bustingorry, W. Savero Torres, J. Gorchon, A. B. Kolton, A. Lemaître, and J.-P. Jamet, Phys. Rev. Lett. **117**, 057201 (2016).

[22] R. Diaz Pardo, W. Savero Torres, A. B. Kolton, S. Bustingorry, and V. Jeudy, Phys. Rev. B **95**, 184434 (2017).

[23] A. I. Larkin, Zh. Eksp. Teor. Fiz. **58**, 1466 (1970).

[24] A. Larkin and Y. N. Ovchinnikov, J. Low Temp. Phys. **34**, 409 (1979).

[25] G. Blatter, M. V. Feigel'man, V. B. Geshkenbein, A. I. Larkin, and V. M. Vinokur, Rev. Mod. Phys. **66**, 1125 (1994).

[26] J. Gorchon, S. Bustingorry, J. Ferré, V. Jeudy, A. B. Kolton, and T. Giamarchi, Phys. Rev. Lett. **113**, 027205 (2014).

[27] A. A. Middleton, Phys. Rev. B **45**, 9465 (1992).

[28] L. Roters, A. Hucht, S. Lübeck, U. Nowak, and K. D. Usadel, Phys. Rev. E **60**, 5202 (1999).

[29] S. Bustingorry, A. B. Kolton, and T. Giamarchi, Europhys. Lett. **81**, 26005 (2008).

[30] S. Bustingorry, A. B. Kolton, and T. Giamarchi, Phys. Rev. B **85**, 214416 (2012).

[31] S. Bustingorry, A. B. Kolton, and T. Giamarchi, Phys. Rev. E **85**, 021144 (2012).

[32] P. Le Doussal, K. J. Wiese, and P. Chauve, Phys. Rev. B **66**, 174201 (2002).

[33] P. J. Metaxas, J. P. Jamet, A. Mougin, M. Cormier, J. Ferré, V. Baltz, B. Rodmacq, B. Dieny, and R. L. Stamps, Phys. Rev. Lett. **99**, 217208 (2007).

[34] E. E. Ferrero, S. Bustingorry, and A. B. Kolton, Phys. Rev. E **87**, 032122 (2013).

[35] A. P. Malozemoff and J. C. Slonczewski, *Magnetic Domain Walls in Bubble Materials: Advances in Materials and Device Research* (Academic Press, New York, 1979), Vol. 1.

[36] A. Dourlat, V. Jeudy, A. Lemaître, and C. Gourdon, Phys. Rev. B **78**, 161303 (2008).

[37] G. S. D. Beach, C. Nistor, C. Knutson, M. Tsoi, and J. L. Erskine, Nature Mater. **4**, 741 (2005).

[38] L. Thevenard, C. Gourdon, S. Haghgoo, J.-P. Adam, H. J. von Bardeleben, A. Lemaître, W. Schoch, and A. Thiaville, Phys. Rev. B **83**, 245211 (2011).

[39] H. E. Stanley, *Introduction to Phase Transitions and Critical Phenomena* (Oxford University Press, Oxford, 1971).

[40] V. Privman, P. Hohenberg, and A. Aharony, in *Phase Transitions and Critical Phenomena*, edited by C. Domb and J. L. Lebowitz (Academic Press, New York, 1991), Vol. 14.

[41] J. Ferré, P. J. Metaxas, A. Mougin, J.-P. Jamet, J. Gorchon, and V. Jeudy, C. R. Phys. **14**, 651 (2013).

[42] T. Nattermann, Y. Shapir, and I. Vilfan, Phys. Rev. B **42**, 8577 (1990).

[43] L.-W. Chen and M. C. Marchetti, Phys. Rev. B **51**, 6296 (1995).

[44] V. Lecomte, S. E. Barnes, J.-P. Eckmann, and T. Giamarchi, Phys. Rev. B **80**, 054413 (2009).

[45] S. Moretti, M. Voto, and E. Martinez, Phys. Rev. B **96**, 054433 (2017).

[46] E. Agoritsas, V. Lecomte, and T. Giamarchi, Phys. Rev. E **87**, 042406 (2013).

[47] A. B. Kolton, A. Rosso, T. Giamarchi, and W. Krauth, Phys. Rev. B **79**, 184207 (2009).

[48] E. Agoritsas, V. Lecomte, and T. Giamarchi, Physica B **407**, 1725 (2012).

[49] M. Voto, L. Lopez-Diaz, and L. Torres, J. Phys. D **49**, 185001 (2016).

[50] E. E. Ferrero, S. Bustingorry, A. B. Kolton, and A. Rosso, C. R. Phys. **14**, 641 (2013).

[51] R. Lavrijsen, D. M. F. Hartmann, A. van den Brink, Y. Yin, B. Barcones, R. A. Duine, M. A. Verheijen, H. J. M. Swagten, and B. Koopmans, Phys. Rev. B **91**, 104414 (2015).

[52] J. P. Pellegren, D. Lau, and V. Sokalski, Phys. Rev. Lett. **119**, 027203 (2017).

[53] *Ferromagnetic Materials: A Handbook on the Properties of Magnetically Ordered Substances*, edited by E. P. Wohlfarth (North-Holland, Amsterdam, 1980), Vol. 2.

[54] S. Haghgoo, M. Cubukcu, H. J. von Bardeleben, L. Thevenard, A. Lemaître, and C. Gourdon, Phys. Rev. B **82**, 041301 (2010).

[55] C. Burrowes, N. Vernier, J.-P. Adam, L. Herrera Diez, K. Garcia, I. Barisic, G. Agnus, S. Eimer, J.-V. Kim, T. Devolder, A. Lamperti, R. Mantovan, B. Ockert, E. E. Fullerton, and D. Ravelosona, Appl. Phys. Lett. **103**, 182401 (2013).

[56] S. Le Gall, N. Vernier, F. Montaigne, M. Gottwald, D. Lacour, M. Hehn, D. Ravelosona, S. Mangin, S. Andrieu, and T. Hauet, Appl. Phys. Lett. **106**, 062406 (2015).

[57] K. Yamada, J.-P. Jamet, Y. Nakatani, A. Mougin, A. Thiaville, T. Ono, and J. Ferré, Appl. Phys. Express **4**, 113001 (2011).

[58] A. Kirilyuk, J. Ferré, V. Grolier, J. P. Jamet, and D. Renard, J. Magn. Magn. Mater. **171**, 45 (1997).